

Observation of large missing-momentum ($e, e'p$) cross-section scaling and the onset of correlated-pair dominance in nuclei

I. Korover,^{1,*} A. W. Denniston,^{1,*} A. Kiral,¹ A. Schmidt,³ A. Lovato,⁶ N. Rocco,⁷ A. Nikolakopoulos,⁷ L. B. Weinstein,⁴ E. Piasetzky,² O. Hen^{1,†}, M. J. Amarian,⁴ Giovanni Angelini,³ H. Atac,⁴⁵ N. A. Baltzell,⁵ L. Barion,²¹ M. Battaglieri,^{5,23} I. Bedlinskiy,³⁴ Fatiha Benmokhtar,¹⁶ A. Bianconi,^{48,27} L. Biondo,^{23,26,49} A. S. Biselli,^{17,10} F. Bossù,¹² S. Boiarinov,⁵ W. J. Briscoe,³ D. Bulumulla,⁴ V. D. Burkert,⁵ D. S. Carman,⁵ J. C. Carvajal,¹⁹ M. Caudron,²⁸ P. Chatagnon,²⁸ T. Chetry,³³ G. Ciullo,^{21,18} L. Clark,⁵⁰ P. L. Cole,^{32,11,5} M. Contalbrigo,²¹ G. Costantini,^{48,27} A. D'Angelo,^{24,42} N. Dashyan,⁵⁴ R. De Vita,²³ M. Defurne,¹² A. Deur,⁵ S. Diehl,^{39,14} C. Djalali,³⁸ M. Duer,⁵⁵ R. Dupre,²⁸ H. Egiyan,⁵ M. Ehrhart,⁶ A. El Alaoui,⁴⁶ L. El Fassi,³³ L. Elouadrhiri,⁵ P. Eugenio,²⁰ S. Fegan,⁵¹ R. Fersch,¹³ A. Filippi,²⁵ G. Gavalian,^{5,35} Y. Ghandilyan,⁵⁴ G. P. Gilfoyle,⁴¹ F. X. Girod,⁵ A. A. Golubenko,⁴³ R. W. Gothe,⁴⁴ K. A. Griffioen,⁵³ M. Guidal,²⁸ L. Guo,^{19,5} K. Hafidi,⁶ H. Hakobyan,^{46,54} M. Hattawy,⁴ T. B. Hayward,¹⁴ D. Heddle,^{13,5} K. Hicks,³⁸ A. Hobart,²⁸ M. Holtrop,³⁵ C. E. Hyde,⁴ Y. Ilieva,^{44,3} D. G. Ireland,⁵⁰ E. L. Isupov,⁴³ H. S. Jo,³¹ K. Joo,¹⁴ S. Joosten,⁶ D. Keller,⁵² A. Khanal,¹⁹ M. Khandaker,^{37,‡} A. Kim,¹⁴ W. Kim,³¹ A. Kripko,³⁹ V. Kubarovsky,^{5,40} L. Lanza,²⁴ M. Leali,^{48,27} P. Lenisa,^{21,18} K. Livingston,⁵⁰ I. J. D. MacGregor,⁵⁰ D. Marchand,²⁸ L. Marsicano,²³ V. Mascagna,^{47,27,§} B. McKinnon,⁵⁰ S. Migliorati,^{48,27} M. Mirazita,²² V. Mokeev,^{5,43} C. Munoz Camacho,²⁸ P. Nadel-Turonski,⁵ K. Neupane,⁴⁴ S. Niccolai,²⁸ G. Niculescu,³⁰ T. R. O'Connell,¹⁴ M. Osipenko,²³ A. I. Ostrovidov,²⁰ P. Pandey,⁴ M. Paolone,³⁶ L. L. Pappalardo,^{21,18} R. Paremuzyan,⁵ E. Pasyuk,⁵ O. Pogorelko,³⁴ M. Pokhrel,⁴ J. W. Poudel,⁴ J. W. Price,⁸ Y. Prok,^{4,52} B. A. Raue,^{19,5} Trevor Reed,¹⁹ M. Ripani,²³ J. Ritman,²⁹ A. Rizzo,^{24,42} G. Rosner,⁵⁰ P. Rossi,⁵ J. Rowley,³⁸ F. Sabatié,¹² R. A. Schumacher,¹⁰ E. P. Segarra,¹ Y. G. Sharabian,⁵ E. V. Shirokov,⁴³ U. Shrestha,¹⁴ O. Soto,²² N. Sparveris,⁴⁵ S. Stepanyan,⁵ I. I. Strakovsky,³ S. Strauch,^{44,3} R. Tyson,⁵⁰ M. Ungaro,^{5,40} L. Venturelli,^{48,27} H. Voskanyan,⁵⁴ A. Vossen,^{15,5} E. Voutier,²⁸ Kevin Wei,¹⁴ X. Wei,⁵ R. Wishart,⁵⁰ M. H. Wood,^{9,44} B. Yale,⁵³ N. Zachariou,⁵¹ J. Zhang,⁵² and Z.W. Zhao¹⁵

(CLAS Collaboration)

¹Massachusetts Institute of Technology, Cambridge, Massachusetts 02139, USA

²School of Physics and Astronomy, Tel Aviv University, Tel Aviv 69978, Israel

³The George Washington University, Washington D.C. 20052, USA

⁴Old Dominion University, Norfolk, Virginia 23529, USA

⁵Thomas Jefferson National Accelerator Facility, Newport News, Virginia 23606, USA

⁶Physics Division, Argonne National Laboratory, Lemont, Illinois 60439, USA

⁷Theoretical Physics Department, Fermi National Accelerator Laboratory, P.O. Box 500, Batavia, Illinois 60510, USA

⁸California State University, Dominguez Hills, Carson, California 90747, USA

⁹Canisius College, Buffalo, New York, USA

¹⁰Carnegie Mellon University, Pittsburgh, Pennsylvania 15213, USA

¹¹Catholic University of America, Washington D.C. 20064, USA

¹²IRFU, CEA, Université Paris-Saclay, F-91191 Gif-sur-Yvette, France

¹³Christopher Newport University, Newport News, Virginia 23606, USA

¹⁴University of Connecticut, Storrs, Connecticut 06269, USA

¹⁵Duke University, Durham, North Carolina 27708-0305, USA

¹⁶Duquesne University, 600 Forbes Avenue, Pittsburgh, Pennsylvania 15282, USA

¹⁷Fairfield University, Fairfield, Connecticut 06824, USA

¹⁸Università di Ferrara, 44121 Ferrara, Italy

¹⁹Florida International University, Miami, Florida 33199, USA

²⁰Florida State University, Tallahassee, Florida 32306, USA

²¹INFN, Sezione di Ferrara, 44100 Ferrara, Italy

²²INFN, Laboratori Nazionali di Frascati, 00044 Frascati, Italy

²³INFN, Sezione di Genova, 16146 Genova, Italy

²⁴INFN, Sezione di Roma Tor Vergata, 00133 Rome, Italy

²⁵INFN, Sezione di Torino, 10125 Torino, Italy

²⁶INFN, Sezione di Catania, 95123 Catania, Italy


*These authors contributed equally to this work.

†Corresponding author: hen@mit.edu

‡Present address: Idaho State University, Pocatello, Idaho 83209, USA

§Present address: Università degli Studi di Brescia, 25123 Brescia, Italy

- ²⁷*INFN, Sezione di Pavia, 27100 Pavia, Italy*
- ²⁸*Universit'e Paris-Saclay, CNRS/IN2P3, IJCLab, 91405 Orsay, France*
- ²⁹*Institute für Kernphysik (Jülich), Jülich, Germany*
- ³⁰*James Madison University, Harrisonburg, Virginia 22807, USA*
- ³¹*Kyungpook National University, Daegu 41566, Republic of Korea*
- ³²*Lamar University, 4400 MLK Blvd, PO Box 10046, Beaumont, Texas 77710, USA*
- ³³*Mississippi State University, Mississippi State, Mississippi 39762-5167, USA*
- ³⁴*National Research Centre Kurchatov Institute - ITEP, Moscow, 117259, Russia*
- ³⁵*University of New Hampshire, Durham, New Hampshire 03824-3568, USA*
- ³⁶*New Mexico State University, PO Box 30001, Las Cruces, New Mexico 88003, USA*
- ³⁷*Norfolk State University, Norfolk, Virginia 23504, USA*
- ³⁸*Ohio University, Athens, Ohio 45701, USA*
- ³⁹*II Physikalisches Institut der Universität Gießen, 35392 Gießen, Germany*
- ⁴⁰*Rensselaer Polytechnic Institute, Troy, New York 12180-3590, USA*
- ⁴¹*University of Richmond, Richmond, Virginia 23173, USA*
- ⁴²*Universita' di Roma Tor Vergata, 00133 Rome, Italy*
- ⁴³*Skobeltsyn Institute of Nuclear Physics, Lomonosov Moscow State University, 119234 Moscow, Russia*
- ⁴⁴*University of South Carolina, Columbia, South Carolina 29208, USA*
- ⁴⁵*Temple University, Philadelphia, Pennsylvania 19122, USA*
- ⁴⁶*Universidad Técnica Federico Santa María, Casilla 110-V Valparaíso, Chile*
- ⁴⁷*Università degli Studi dell'Insubria, 22100 Como, Italy*
- ⁴⁸*Universit'a degli Studi di Brescia, 25123 Brescia, Italy*
- ⁴⁹*Universit'a degli Studi di Messina, 98166 Messina, Italy*
- ⁵⁰*University of Glasgow, Glasgow G12 8QQ, United Kingdom*
- ⁵¹*University of York, York YO10 5DD, United Kingdom*
- ⁵²*University of Virginia, Charlottesville, Virginia 22901, USA*
- ⁵³*College of William and Mary, Williamsburg, Virginia 23187-8795, USA*
- ⁵⁴*Yerevan Physics Institute, 375036 Yerevan, Armenia*
- ⁵⁵*Technische Universität Darmstadt, Fachbereich Physik, Darmstadt, Germany*

 (Received 4 September 2022; revised 29 November 2022; accepted 26 May 2023; published 6 June 2023)

We report the measurement of x_B scaling in $(e, e'p)$ cross-section ratios off nuclei relative to deuterium at large missing momentum of $350 \leq p_{\text{miss}} \leq 600$ MeV/ c . The observed scaling extends over a kinematic range of $0.7 \leq x_B \leq 1.8$, which is significantly wider than $1.4 \leq x_B \leq 1.8$ previously observed for inclusive (e, e') cross-section ratios. The x_B -integrated cross-section ratios become constant (i.e., scale) beginning at $p_{\text{miss}} \approx k_F$, the nuclear Fermi momentum. Comparing with theoretical calculations we find good agreement with generalized contact formalism calculations for high missing momentum (>375 MeV/ c), suggesting the observed scaling results from interacting with nucleons in short-range correlated (SRC) pairs. For low missing momenta, mean-field calculations show good agreement with the data for $p_{\text{miss}} < k_F$, and suggest a potential non-negligible contribution to the measured cross-section ratios from scattering off single, uncorrelated, nucleons up to $p_{\text{miss}} \approx 350$ MeV/ c . Therefore, SRCs become dominant in nuclei at $p_{\text{miss}} \approx 350$ MeV/ c , well above the nuclear Fermi Surface of $k_F \approx 250$ MeV/ c .

DOI: [10.1103/PhysRevC.107.L061301](https://doi.org/10.1103/PhysRevC.107.L061301)

Atomic nuclei are among the fundamental building blocks of the visible universe. The complexity of the strong nuclear interaction makes it difficult to use scattering reactions to experimentally probe the detailed distributions of nucleons inside nuclei. Experimental nuclear physicists thus work together with theorists to find measurable reactions that are sensitive to particular aspects of nuclear dynamics.

By using high-energy electron beams to knock out nucleons from nuclei in nearly elastic kinematics, one can learn about the behavior of single nucleons in the nucleus [1]. This behavior can be generally explained by nucleons moving in

nuclear shell-model states (e.g., s , p , d ,) where the typical nucleon momenta in each shell is smaller than the nuclear Fermi momentum (k_F). Full shell-model calculations improve on this by introducing effective long-ranged correlations between the nucleons [2], which leads to the formation of a nuclear Fermi surface.

While these models can successfully describe the long-range structure of nuclei, they do not describe the explicit high-resolution effects of short-range correlated (SRC) nucleon pairs. Within a high-resolution picture of nuclear dynamics, SRC pairs arise when two nucleons get so close

to each other that the short-range nuclear interaction between them is much stronger than the effective long-ranged nuclear mean field due to their interactions with all the other nucleons in the nucleus [3,4].

SRCs have been clearly identified in data using large momentum-transfer nucleon knockout reactions [5–9]. They are characterized by a high (greater than k_F) relative momentum between the nucleons of the pair and are predominantly proton-neutron pairs formed due to the action of the spin-dependent tensor part of the strong nuclear interaction [10–13]. They thus deplete the occupancy of single-particle shell-model states (below k_F) and populate high-momentum states [3,4,9,14–16]. While shell structures vary among nuclei, SRCs are a universal phenomenon, i.e., they are similar in all nuclei [4,17–19], varying primarily in their magnitude.

A complete high-resolution microscopic description of atomic nuclei should thus start with the nucleus-dependent mean field and long-ranged nuclear shell model parts as well as explicit nucleus-independent effects of SRC pairs.

Here, we study the onset of SRC dominance in semi-inclusive high-energy electron scattering reactions, where we detect the knocked-out proton in addition to the scattered electron, ($e, e'p$). We observed scaling in the cross-section ratios of nuclei from carbon to lead relative to deuterium over a broad range in the Bjorken scaling variable, x_B . This scaling substantially extends the kinematical range where SRCs can be identified and studied, as compared with previous inclusive (e, e') measurements. Thereby, they provide direct experimental evidence for the dominance SRCs in the scattering response at high missing momenta, and allow quantifying the onset of this dominance.

Our experiment ran at the Thomas Jefferson National Accelerator Facility. It used a 5.01 GeV electron beam incident on a target system consisting of a deuterium cell followed by an interchangeable solid foil of carbon (C), aluminum (Al), iron (Fe), or lead (Pb) [20]. Scattered electrons and knocked-out protons were identified and measured using the CEBAF Large Acceptance Spectrometer (CLAS) [21] (see [36] for details).

In high-energy scattering, the electron transfers a single virtual photon to the nucleus with momentum \vec{q} and energy ω . In the high-resolution quasielastic (QE) reaction picture, the virtual photon is absorbed by a single nucleon, which gets knocked-out of the nucleus with momentum \vec{p}_p . By measuring both the scattered electron and knocked-out proton, i.e., the ($e, e'p$) reaction, we can determine the missing momentum $\vec{p}_{\text{miss}} = \vec{p}_p - \vec{q}$. The reaction is further characterized by the four-momentum transfer $Q^2 = \vec{q}^2 - \omega^2$ and Bjorken scaling variable $x_B = Q^2/2m\omega$, where m is the nucleon mass.

If the knocked-out nucleon does not re-interact as it leaves the nucleus, then \vec{p}_{miss} is equal to the initial momentum of that nucleon. Thus we expect the reaction to be sensitive to mean-field nucleons at low- p_{miss} and to SRCs at high- p_{miss} [22]. In the SRC dominated region, the cross section ratio for any two nuclei should be constant (i.e., independent of p_{miss}) and equal to the relative number of high-momentum nucleons in the two nuclei [4,9,14,23–26]. Thus, by measuring the ($e, e'p$) cross section ratio for nuclei relative to deuterium for different minimum p_{miss} , we can establish the onset of

scaling that corresponds to SRC pair dominance in the nuclear momentum distribution.

To study this, we measured the ($e, e'p$) reaction in conditions sensitive to the knockout of protons from SRC pairs. We required $Q^2 \geq 1.5$ (GeV/c)² and $350 \leq p_{\text{miss}} \leq 600$ MeV/c to ensure a high-resolution reaction that can resolve single nucleons in SRC pairs. We further required that the proton be emitted within 25° of the momentum transfer, to ensure that the measured proton was the nucleon that absorbed the virtual photon [7,27].

We suppressed inelastic (non-QE) scattering events by requiring M_{miss} , the missing mass for ($e, e'p$) scattering from a two-nucleon pair at rest, to be smaller than the nucleon mass (m) plus pion mass (m_π), $0.8 \leq M_{\text{miss}} \leq m + m_\pi = 1.08$ GeV/c². In non-QE reactions the momentum transferred to undetected particles (e.g., pions) shifts the direction of \vec{p}_{miss} . Therefore such events will have a larger $\theta_{\vec{p}_{\text{miss}}, \vec{q}}$, the angle between \vec{p}_{miss} and \vec{q} . We thus further suppressed the small non-QE tail below $M_{\text{miss}} = 1.08$ GeV/c² by observing that the measured $\theta_{\vec{p}_{\text{miss}}, \vec{q}}$ distribution has two maxima, corresponding to QE and non-QE scattering, and selecting events in the $\theta_{\vec{p}_{\text{miss}}, \vec{q}}$ QE peak. This small angle selection also allows suppression of final state interactions (FSI) that, at these large Q^2 , primarily scatter the protons into perpendicular kinematics [11,28,29]. See Figs. S1 and S2 and the Supplemental Material for details [36].

We tested our identification of scattering from protons in SRC pairs by comparing the measured width of the M_{miss} peak with that calculated using the generalized contact formalism (GCF) model for SRC pairs (see Fig. 1) [8,19,27,30–32]. This width depends on the CLAS resolution and on the SRC pair center of mass (c.m.) motion. We corrected for the effects of the CLAS resolution by subtracting the deuterium M_{miss} peak width from that of ¹²C to get the intrinsic width: $\sigma_{\text{int}}^{12\text{C}} = \sqrt{(\sigma_{\text{exp}}^{12\text{C}})^2 - (\sigma_{\text{exp}}^d)^2}$.

The measured x_B dependence of $\sigma_{\text{int}}^{12\text{C}}$ agrees well with a GCF calculation that assumes electron scattering from nucleons in SRC pairs with a realistic Gaussian c.m. momentum distribution [33], as was done in Refs. [8,27,30]. The calculation accounts for the CLAS detector acceptance and resolution and our event selection cuts. The width of the c.m. momentum distributions, $\sigma_{\text{c.m.}}$, and the excitation energy of the residual nuclear system after the SRC breakup, E^* , were the only two free parameters used in the calculation and were determined from a fit of the calculation to the data (see inset of Fig. 1). For $\sigma_{\text{c.m.}}$ the fitted values of 160–210 MeV/c (125–220) at 68% (90%) confidence agree well with previous direct measurements [8,33]. For E^* , while not previously measured, the fitted values of 20–55 MeV (0–70 MeV) at 68% (90%) confidence are consistent with those used by previous analyses [27]. The sensible values of the resulting fit parameters and the agreement between the x_B dependence of the GCF calculation and the data further support our interpretation of the data as dominated by scattering off SRC pairs and that the effects of FSI (which would broaden the distribution) are relatively small.

Using the selected event samples, we extracted the ($e, e'p$) cross section ratios for scattering off the solid targets

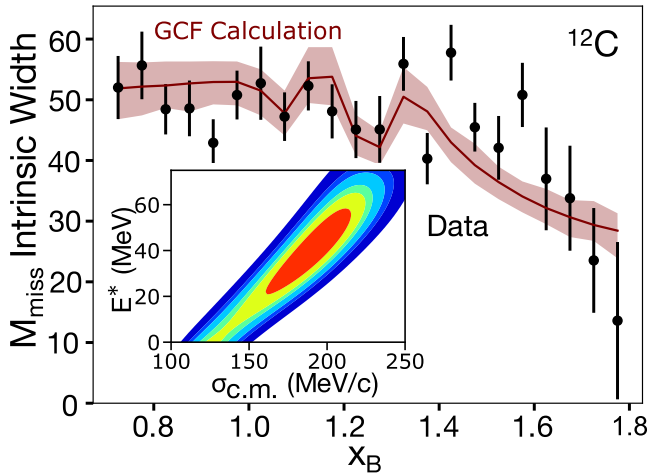


FIG. 1. The intrinsic width of the ^{12}C missing mass (M_{miss}) distribution, plotted vs x_B . Black points show the data. The red curve and uncertainty band shows an SRC based generalized contact formalism (GCF) calculation [19,30]. The two main model parameters of the calculation, namely SRC pair c.m. momentum distribution width $\sigma_{c.m.}$ and the residual $A - 2$ system excitation energy E^* , are fit to the data. Data error bars and calculation error band show the total uncertainty (statistical + systematic) at the 1σ or 68% confidence level. Inset: The resulting confidence intervals of the correlation between the fitted values of $\sigma_{c.m.}$ and E^* . The inner region (red) shows the 1σ (68%) confidence region with each region increasing the confidence by an additional 1σ . The observed agreement between the data and GCF calculation, and the agreement of the fitted model parameters with previous extractions, show the measured $(e, e'p)$ events are consistent with resulting from the hard breakup of SRC pairs.

relative to deuterium. We first divided the ratio of the measured numbers of events for a given target to deuterium with the ratio of the experimentally determined integrated luminosities to obtain the normalized-yield ratios. We then determined the cross section ratios by correcting the normalized-yield ratios for attenuation of the outgoing protons as they traverse the different nuclei [34], electron radiation effects, and the small difference in the CLAS acceptance for detecting particles emitted from the deuterium and the solid targets. At the large Q^2 of this measurement, the attenuation correction is less sensitive to the initial nucleon momenta and therefore both mean-field and SRC breakup reactions have the same attenuation [34]. Acceptance effects were calculated using the CLAS detector simulation [35] and an electron scattering reaction event generator based on the GCF as applied in previous studies [27,30] (see [36] for details).

Figure 2 shows the per nucleon $(e, e'p)$ cross section ratios for $350 \leq p_{\text{miss}} \leq 600$ MeV/c for carbon, aluminum, iron, and lead relative to deuterium as a function of x_B . The $(e, e'p)$ ratios scale (i.e., are constant) for all four nuclei over the entire measured x_B range. This implies that the reaction is probing similar nuclear configurations in the measured nuclei and in deuterium. As the deuteron is a simple proton-neutron correlated two-body system, we interpret this high

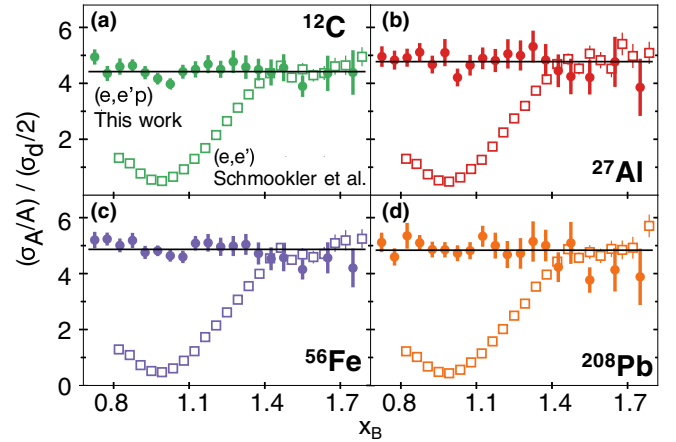


FIG. 2. Measured $(e, e'p)$ per nucleon cross-section ratios for $350 \leq p_{\text{miss}} \leq 600$ MeV/c for carbon, aluminum, iron, and lead relative to deuterium as function of x_B . Open squares are the inclusive (e, e') per nucleon cross section ratios of Ref. [26]. The horizontal lines show the average (e, e') cross section ratio for $1.45 \leq x_B \leq 1.8$ [26]. Error bars show the data uncertainty (statistical plus point-to-point systematic) at the 1σ or 68% confidence level. Overall $(e, e'p)$ systematic uncertainties of 10% (C) to 15% (Pb) are not shown.

missing-momentum scaling as observation of deuteron-like proton-neutron SRC pairs in nuclei. The cross-section ratio is thus a measure of their relative abundance.

This interpretation is supported by the consistency between our measured $(e, e'p)$ cross section ratios and previously measured inclusive (e, e') scattering cross section ratios at similar Q^2 and at $x_B \geq 1.5$ [14,23–26] (see open symbols in Fig. 2). As the inclusive scaling onset at $x_B \approx 1.5$ has been attributed to scattering off nucleons with momenta greater than ≈ 275 MeV/c [14,37], it is also associated with scattering off nucleons in deuteron-like proton-neutron SRC pairs, formed by the strong tensor interaction [23,26] (see [36] for details). Proton detection extends the cross-section ratio plateau down to $x_B = 0.7$, providing a new experimental tool to study the transition to SRC dominance in nuclei over a broad range in x_B .

We next examined how this scaling depends on the minimum p_{miss} range of the data. Figure 3 (left) shows the per nucleon $(e, e'p)$ cross section ratios for carbon relative to deuterium as a function of x_B for different minimum p_{miss} . Results for the other measured nuclei are shown in Fig. 4. For all nuclei, the curve for $p_{\text{miss}}^{\text{min}} = 0$ are similar to the inclusive data of Schmockler *et al.* [26], with a plateau for $x_B \geq 1.5$ and a minimum at $x_B \approx 1$. As $p_{\text{miss}}^{\text{min}}$ increases, this minimum fills in. For $p_{\text{miss}}^{\text{min}} \gtrsim 200$ –250 MeV/c, it is completely filled in and the $(e, e'p)$ cross section ratio scales over the full measured x_B range of 0.7 to 1.8. This indicates that short-range interactions become dominant at around $k_F \approx 220$ –260 MeV/c [38], as expected.

To better quantify this transition, Fig. 3 (right) shows the p_{miss} dependence of the $(e, e'p)$ cross section ratio for carbon relative to deuterium, integrated over the scaling regions of $0.7 \leq x_B \leq 1.8$ (see Fig. 4 for the same results for the other

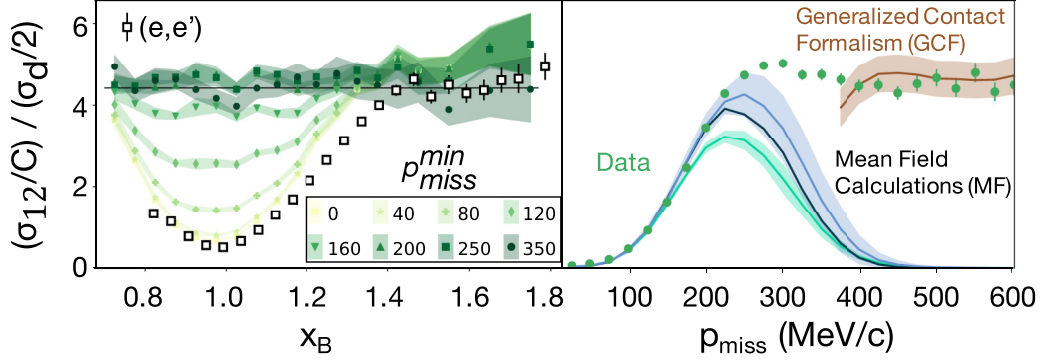


FIG. 3. The per-nucleon cross-section ratios for carbon relative to deuterium as a function of x_B (left) and p_{miss} (right). In the left panel full symbols with different colors indicate different lower limits of the p_{miss} integration. The upper p_{miss} limit is fixed at 600 MeV/c. The colored bands mark the statistical plus point-to-point systematical uncertainty of the data at the $\pm 1\sigma$ or 68% confidence level. Open black squares show the inclusive (e, e') per nucleon cross-section ratios of Ref. [26]. The horizontal line shows the average (e, e') cross section ratio for $1.45 \leq x_B \leq 1.8$ [26]. In the right panel the cross-section ratios are integrated over $0.7 \leq x_B \leq 1.8$. Filled circles show the data. The brown line shows calculated cross sections for scattering off SRC nucleons in carbon using the GCF model while the other lines show calculations for one-body mean-field nucleons obtained using QMC (teal), IPSM (black), and Skyrme (azure) models. Data error bars and the widths of the bands around the calculation lines show their uncertainties (statistical plus point-to-point systematical) at the 1σ or 68% confidence level. In both panels overall data systematic data uncertainties of 10–15 % are not shown.

measured nuclei). The measured cross section ratio for carbon ($k_F \approx 220$ MeV/c), aluminum ($k_F \approx 235$ MeV/c), and iron ($k_F \approx 260$ MeV/c) all become flat starting around the Fermi momentum at $p_{\text{miss}} \approx 250$. The lead ratio shows a similar transition but does not fully plateau, possibly owing to its much larger neutron-to-proton ratio or to increased final state interactions due to its larger size. Improved reaction calculations and future $(e, e'n)$ cross-section ratio measurements will allow disentangling the size and asymmetry effects to better understand the observed behavior in lead.

We thus conclude that the data indicate the existence of a clear transition in the nuclear response around the nuclear

Fermi momentum, caused by the onset of SRC dominance at high momenta.

Focusing on the carbon nucleus, where theoretical calculations are readily available, we find that the high- p_{miss} data are in excellent agreement with an asymptotic GCF calculation of the cross-section ratio (brown band in Fig. 3, right panel). The calculation was done using a factorized plane-wave impulse approximation (PWIA) for the scattering reaction, with SRC-pair spectral functions calculated using the GCF [39] and transparency and single-charge exchange corrections as done in Refs. [27,30,40] (see [36] for details). The SRC-pair abundance parameters used by the GCF calculation were all previously determined by *ab initio* many-body theoretical calculations [19], offering additional support to our identification of QE scattering events and the dominance of interacting with nucleons in SRC pairs at high- p_{miss} .

Lastly, we estimate the possible contribution of single-nucleon (one-body) states to the measured cross-section ratio at or below k_F . We examined three calculations using different single-nucleon spectral functions: (1) Independent particle shell-model with a Woods-Saxon potential [41,42], (2) Skyrme model using five different functionals [43,44], and (3) new quantum Monte Carlo (QMC) many-body calculations of the overlap between the ^{12}C and $^{11}\text{B} + \text{proton}$ wave functions (see [36] for details). For the latter, we summed the contributions from both the ^{11}B ground state and a range of excited states to include a wide range of mean-field, single-nucleon states. These models each assume very different underlying single-body nuclear dynamics, and thus the spread in their results offers a general measure for the model dependence of the single-body mean-field contribution.

These mean-field contributions to the carbon to deuterium $(e, e'p)$ cross-section ratio are shown in Fig. 3 (right). The calculations were done using the same factorized PWIA scheme as for the GCF calculation, only using mean-field spectral functions. The IPSM and Skyrme calculations are

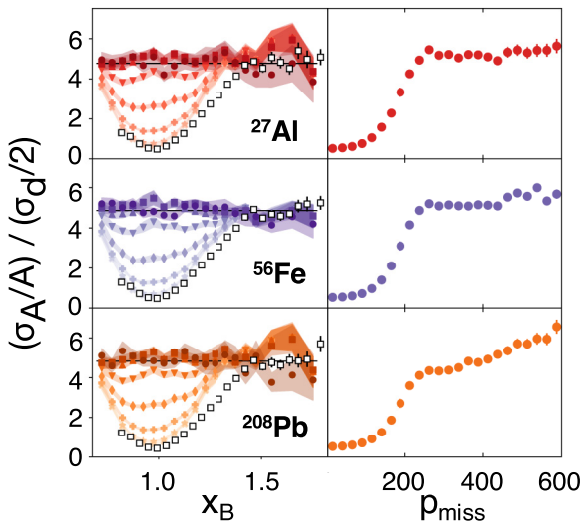


FIG. 4. Same as Fig. 3, for the cross-section ratio of aluminum, iron, and lead relative to deuterium and shown as a function of x_B (left) and p_{miss} (right).

renormalized (quenched) to agree with the data at low- $p_{\text{miss}} (\leq 150 \text{ MeV}/c)$. This quenching effectively accounts for the depletion of single-nucleon strength due to long- and short-ranged correlations and/or few-body reaction operators [45]. In contrast, the QMC calculation extracts the underlying single-nucleon states from the fully correlated high-resolution wave function. It thus has fewer than six protons in its mean-field orbitals and does not require additional quenching. The agreement of the QMC calculation with the low- p_{miss} data thus confirms the completeness of the calculation.

The different single-nucleon calculations are similar, well reproducing the data below k_F and indicating the possible existence of residual single nucleon contributions above k_F . As the transition region between the pure mean-field to the pure SRC regions includes contributions from both single-nucleon and two-nucleon knockout mechanisms, its theoretical description can be more complex and require a more detailed treatment than the one employed here. Future theoretical calculations will therefore be able to use our data to map in detail the transition from the mean-field to SRC regime, which seems to occur above k_F at about $\approx 350\text{--}400 \text{ MeV}/c$.

To conclude, the new nuclear scaling measurements presented herein allow isolating interactions with SRC pairs in a substantially extended kinematical regime. By examining the scaling onset in missing momentum, we observe a transition in the scattering response above the nuclear Fermi momentum. This transition leads to a level plateau in carbon, aluminum and iron and a significant slope change in lead. Using model dependent estimates for the individual SRC and

mean field contributions, we see an indication for the onset of full SRC dominance above $\approx 350\text{--}400 \text{ MeV}/c$. Detailed theoretical calculations will be able to use our data to fully quantify this mean-field to SRC transition region and to obtain an effective high-resolution description of a wide range of heavy nuclei.

The ability to establish SRC scaling at low- x_B with the $(e, e'p)$ reaction allows for high counting-rate SRC measurements using both $(e, e'p)$ and $(e, e'n)$ reactions. Such future studies will provide a new method for high-precision probes of SRC dynamics in neutron-rich nuclei.

We acknowledge the efforts of the staff of the Accelerator and Physics Divisions at Jefferson Laboratory that made this experiment possible. The analysis presented here was carried out as part of the Jefferson Lab Hall B data-mining project supported by the U.S. Department of Energy (DOE). The research was also supported by the National Science Foundation, the Israel Science Foundation, the Pazi Foundation, the Chilean Comisión Nacional de Investigación Científica y Tecnológica, the French Centre National de la Recherche Scientifique and Commissariat à l'Énergie Atomique, the FrenchAmerican Cultural Exchange, the Italian Istituto Nazionale di Fisica Nucleare, the National Research Foundation of Korea, and the UK Science and Technology Facilities Council. Jefferson Science Associates operates the Thomas Jefferson National Accelerator Facility for the DOE, Office of Science, Office of Nuclear Physics under Contract No. DE-AC05-06OR23177.

-
- [1] J. Kelly, *Adv. Nucl. Phys.* **23**, 75 (1996).
 [2] W. H. Dickhoff and C. Barbieri, *Prog. Part. Nucl. Phys.* **52**, 377 (2004).
 [3] L. Frankfurt and M. Strikman, *Phys. Rep.* **160**, 235 (1988).
 [4] C. Ciofi degli Atti, *Phys. Rep.* **590**, 1 (2015).
 [5] A. Tang *et al.*, *Phys. Rev. Lett.* **90**, 042301 (2003).
 [6] R. Subedi *et al.*, *Science* **320**, 1476 (2008).
 [7] O. Hen *et al.*, *Science* **346**, 614 (2014).
 [8] M. Patsyuk *et al.* (BM@N Collaboration), *Nat. Phys.* **17**, 693 (2021).
 [9] O. Hen, G. A. Miller, E. Piassetzky, and L. B. Weinstein, *Rev. Mod. Phys.* **89**, 045002 (2017).
 [10] R. Schiavilla, R. B. Wiringa, S. C. Pieper, and J. Carlson, *Phys. Rev. Lett.* **98**, 132501 (2007).
 [11] M. M. Sargsian, T. V. Abrahamyan, M. I. Strikman, and L. L. Frankfurt, *Phys. Rev. C* **71**, 044615 (2005).
 [12] M. Alvioli, C. Ciofi degli Atti, and H. Morita, *Phys. Rev. Lett.* **100**, 162503 (2008).
 [13] T. Neff, H. Feldmeier, and W. Horiuchi, *Phys. Rev. C* **92**, 024003 (2015).
 [14] K. Egiyan *et al.* (CLAS Collaboration), *Phys. Rev. Lett.* **96**, 082501 (2006).
 [15] S. Paschalis, M. Petri, A. O. Macchiavelli, O. Hen, and E. Piassetzky, *Phys. Lett. B* **800**, 135110 (2020).
 [16] J. Ryckebusch, W. Cosyn, T. Viejra, and C. Casert, *Phys. Rev. C* **100**, 054620 (2019).
 [17] C. Ciofi degli Atti and S. Simula, *Phys. Rev. C* **53**, 1689 (1996).
 [18] J. Ryckebusch, M. Vanhalst, and W. Cosyn, *J. Phys. G: Nucl. Part. Phys.* **42**, 055104 (2015).
 [19] R. Cruz-Torres *et al.*, *Nat. Phys.* **17**, 306 (2021).
 [20] H. Hakobyan *et al.*, *Nucl. Instrum. Methods Phys. Res. A* **592**, 218 (2008).
 [21] B. A. Mecking *et al.*, *Nucl. Instrum. Methods Phys. Res. A* **503**, 513 (2003).
 [22] M. Duer *et al.* (CLAS Collaboration), *Nature (London)* **560**, 617 (2018).
 [23] L. L. Frankfurt, M. I. Strikman, D. B. Day, and M. Sargsyan, *Phys. Rev. C* **48**, 2451 (1993).
 [24] K. Egiyan *et al.* (CLAS Collaboration), *Phys. Rev. C* **68**, 014313 (2003).
 [25] N. Fomin *et al.*, *Phys. Rev. Lett.* **108**, 092502 (2012).
 [26] B. Schmookler *et al.* (CLAS Collaboration), *Nature (London)* **566**, 354 (2019).
 [27] A. Schmidt *et al.* (CLAS Collaboration), *Nature (London)* **578**, 540 (2020).
 [28] L. L. Frankfurt, M. M. Sargsian, and M. I. Strikman, *Phys. Rev. C* **56**, 1124 (1997).
 [29] M. M. Sargsian *et al.*, *J. Phys. G: Nucl. Part. Phys.* **29**, R1 (2003).
 [30] J. Pybus, I. Korover, R. Weiss, A. Schmidt, N. Barnea, D. Higinbotham, E. Piassetzky, M. Strikman, L. Weinstein, and O. Hen, *Phys. Lett. B* **805**, 135429 (2020).
 [31] R. Weiss, B. Bazak, and N. Barnea, *Phys. Rev. C* **92**, 054311 (2015).

- [32] R. Weiss, R. Cruz-Torres, N. Barnea, E. Piasetzky, and O. Hen, *Phys. Lett. B* **780**, 211 (2018).
- [33] E. O. Cohen *et al.* (CLAS Collaboration), *Phys. Rev. Lett.* **121**, 092501 (2018).
- [34] M. Duer *et al.* (CLAS Collaboration), *Phys. Lett. B* **797**, 134792 (2019).
- [35] E. Wolin, CLAS - GEANT simulation, 1996, URL <https://www.jlab.org/Hall-B/document/gsim/userguide.html>.
- [36] See Supplemental Material at <http://link.aps.org/supplemental/10.1103/PhysRevC.107.L061301> for additional analysis details.
- [37] R. Weiss, A. W. Denniston, J. R. Pybus, O. Hen, E. Piasetzky, A. Schmidt, L. B. Weinstein, and N. Barnea, *Phys. Rev. C* **103**, L031301 (2021).
- [38] E. J. Moniz, I. Sick, R. R. Whitney, J. R. Ficenec, R. D. Kephart, and W. P. Trower, *Phys. Rev. Lett.* **26**, 445 (1971).
- [39] R. Weiss, I. Korover, E. Piasetzky, O. Hen, and N. Barnea, *Phys. Lett. B* **791**, 242 (2019).
- [40] M. Duer *et al.* (CLAS Collaboration), *Phys. Rev. Lett.* **122**, 172502 (2019).
- [41] T. O'Neill, W. Lorenzon, P. Anthony, R. Arnold, J. Arrington, E. Beise, J. Belz, P. Bosted, H.-J. Bulten, M. Chapman *et al.*, *Phys. Lett. B* **351**, 87 (1995).
- [42] N. Makins *et al.*, *Phys. Rev. Lett.* **72**, 1986 (1994).
- [43] M. Waroquier, J. Sau, K. Heyde, P. Van Isacker, and H. Vincx, *Phys. Rev. C* **19**, 1983 (1979).
- [44] E. Chabanat, P. Bonche, P. Haensel, J. Meyer, and R. Schaeffer, *Nucl. Phys. A* **635**, 231 (1998); [Erratum: **643**, 441 (1998)].
- [45] A. J. Tropiano, S. K. Bogner, and R. J. Furnstahl, *Phys. Rev. C* **104**, 034311 (2021).